JACS Au
AN OPEN ACCESS JOURNAL OF THE AMERICAN CHEMICAL SOCIETY

pubs.acs.org/jacsau
Article

Mechanistic Insights into Nonadiabatic Interband Transitions on a Semiconductor Surface Induced by Hydrogen Atom Collisions

Lingjun Zhu, Qijing Zheng, Yingqi Wang, Kerstin Krüger, Alec M. Wodtke, Oliver Bünermann, Jin Zhao,* Hua Guo,* and Bin Jiang*

Cite This: *JACS Au* 2024, 4, 4518−4526

ABSTRACT: To understand the recently observed enigmatic nonadiabatic energy transfer for hyperthermal H atom scattering from a semiconductor surface, Ge(111)$c(2 \times 8)$, we present a mixed quantum-classical nonadiabatic molecular dynamics model based on the time-dependent evolution of Kohn−Sham orbitals and a classical path approximation. Our results suggest that facile nonadiabatic electronic transitions from the valence band to the conduction band occur selectively at the rest atom site, where surface states are doubly occupied, but not at the adatom site, where empty surface states are localized. This drastic site specificity can be attributed to the changes of the local band structure upon energetic H collisions at different surface sites, leading to transient near degeneracies and significant couplings between occupied and unoccupied orbitals at the rest atom but not at the adatom. These insights shed valuable light on the collision-induced nonadiabatic dynamics at semiconductor surfaces.

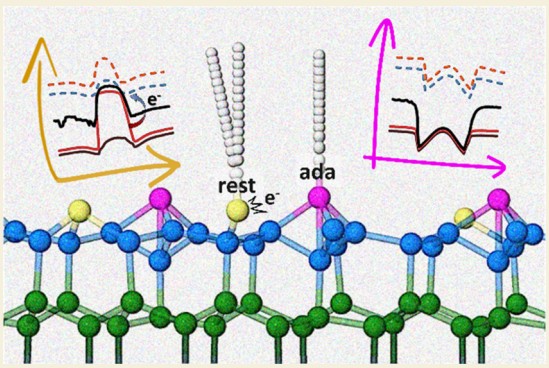

KEYWORDS: *surface scattering, nonadiabatic molecular dynamics, site specificity, interband electronic transitions, semiconductor surface*

I. INTRODUCTION

The Born−Oppenheimer approximation (BOA),[1] which assumes much faster electronic motion than nuclear motion, represents a key construct for understanding spectroscopy and collision dynamics. This approximation is however known to break down when two or more electronic states are energetically close to each other. The resulting nonadiabatic effects are of fundamental importance in chemistry, ranging from photochemistry in the atmosphere, electron transfer processes in solutions, to electrochemistry at interfaces. For gas phase systems, where electronic degeneracies are infrequent, the breakdown of BOA is reasonably well understood and various theoretical methods for treating nonadiabatic dynamics have been developed.[2−7] In solids and at surfaces, where nonadiabatic effects have profound implications in plasmonic catalysis and photoelectrochemical applications,[8,9] however, the relevant mechanisms for the breakdown of BOA remain largely unexplored until recently.

Recent experiments have started to examine nonadiabatic processes on metal surfaces, in which a large number of electronic states exist with infinitesimal energy differences. As a result, the breakdown of BOA is found to be more prevalent.[10,11] Indeed, a range of electronically nonadiabatic phenomena, such as efficient vibrational quenching,[12,13] electron emission,[14] chemicurrents,[15] and collisional energy dissipation,[16] have been reported when atoms/molecules interact with metal surfaces. These behaviors can often be interpreted in terms of instantaneous formation of electron−hole pairs (EHPs) due to the coupling of metallic electrons with nuclear motion through formation of a transient anion, or arising from an electronic frictional (EF) force on nuclear motion.[17] The ready breakdown of BOA on metal surfaces is in sharp contrast with their insulator counterparts, in which the large band gap prevents electronic excitation between the valence band (VB) and conduction band (CB).[16,18]

Very recently, nonadiabatic effects have been reported on semiconductor surfaces. As an intermediate case between insulators and conductors, semiconductors have a significant energy gap between VB and CB that cannot be easily overcome by thermal excitation. By impinging hyperthermal H/D on a reconstructed Ge(111)$c(2 \times 8)$ surface, Krüger et al. measured the energy loss of the scattered projectiles at different incidence energies.[19] For an incidence energy below the band gap, there is only one peak in the energy loss distribution. This distribution, along with the corresponding angular distribution of the scattered H, was accurately reproduced by adiabatic molecular dynamics,[19] signaling its

Received: September 27, 2024
Revised: November 5, 2024
Accepted: November 5, 2024
Published: November 14, 2024

https://doi.org/10.1021/jacsau.4c00909
JACS Au 2024, 4, 4518−4526

mechanical nature. When the incidence energy is above the band gap, however, two peaks were found. Again, one peak can be successfully modeled with adiabatic molecular dynamics; however, the second peak exhibiting a large energy loss cannot be accounted for by any existing model. Interestingly, the threshold coincides with the surface band gap (0.49 ± 0.03 eV[20]), prompting the obvious conclusion that the large energy loss peak is due to nonadiabatic excitation of substrate electrons induced by the energetic collision of the fast atomic hydrogen.[19] A recent work with deuterium atoms scattering from the same surface revealed the same energy loss pattern as hydrogen atoms, which was speculated to be due to strong site specificity of nonadiabatic effects.[21]

Naturally, the situation here is quite different from metals, where an EHP excitation is relatively easy and delocalized due to the lack of a band gap, and as a result the perturbation to the nuclear motion can be approximated by the EF theory.[22−24] For the Ge surface, the interband transition across a large band gap of approximately 0.5 eV induced by the incidence of H/D requires a completely new theoretical framework. In the original publication,[19] the authors speculated that the nonadiabatic transition can be likened to a localized curve crossing between two electronic states in a gaseous system. The EF model was found unable to reproduce the experimental observations,[19] which clearly indicate its incapability of treating localized excitation of EHPs due to collisions from semiconductor surfaces. Indeed, a large number of electronic states in the VB and the CB need to be modeled if a first-principles characterization is to be established. Currently, such a theory does not exist, although recent band structure calculations have provided some hints on the origin of the site specificity.[21] As depicted in Figure 1, there are three types of surface atoms on the reconstructed Ge(111), namely the adatoms, the rest atoms, and the saturated atoms, respectively. Their disparate coordination numbers make their interactions with the hydrogen atom distinct. It is thus intriguing to investigate the correlation between their local electronic structures and the nonadiabatic effects.

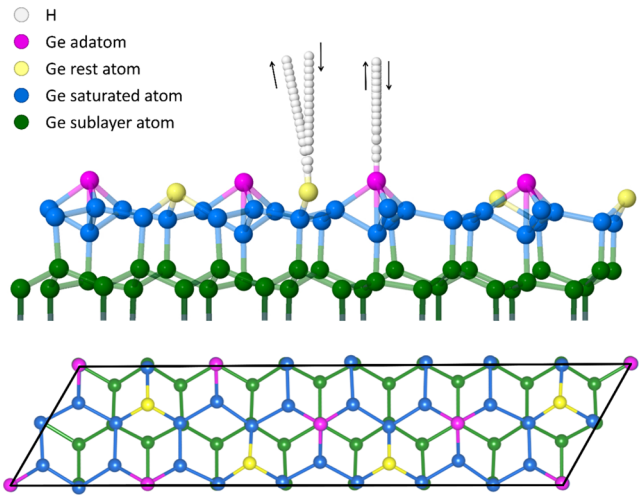

Figure 1. Schematics of two exemplary trajectories of H (white) collisions with a reconstructed Ge(111)$c(2 \times 8)$ surface at a Ge adatom (magenta) and a Ge rest atom (yellow) in a side view. A top view of the clean surface is also included for showing the site positions.

To this end, in this work, we analyze the change in the band structure of Ge(111)$c(2 \times 8)$ upon the adsorption of H on different surface sites and extract information about charge transfer and spin polarization. Furthermore, we follow explicitly the electronic dynamics during the direct scattering of H atoms off these sites by time-dependent nonadiabatic molecular dynamics (NAMD) simulations based on Kohn−Sham (KS) orbitals. While such simulations cannot model the experiment directly, clear and strong site-specific nonadiabatic effects are revealed, which support the curve-crossing hypothesis recently proposed.[19,21] It is found that such curve-crossings are present when H atoms collide at the Ge rest atom site, most likely leading to interband transitions from the VB to the CB, while not at the Ge adatom site. The theoretical studies reported here thus advance our understanding of the newly discovered nonadiabatic effects in surface dynamics.

II. METHODS

Spin-polarized plane-wave DFT calculations were performed with the Vienna Ab initio Simulation Package (VASP).[25] The core electron-nuclei interaction was described by the projector augmented wave (PAW) method[26] and the KS wave function was expanded in plane waves with an energy cutoff of 400 eV. The reconstructed Ge(111) surface was represented by a slab in a $c(2 \times 8)$ supercell with the size of 8.0 × 32.0 Å plus a vacuum space of 16 Å in the z direction to avoid artificial interslab interactions. Each slab contains eight atomic layers, with four additional Ge adatoms exposed on the topmost layer, as illustrated in Figure 1. The Ge adatoms, along with the upper six layers—including rest atoms and saturated atoms—were allowed to move, while the bottom two layers were fixed in its equilibrium positions and passivated by H atoms. A Γ-centered k-point grid of (6 × 1 × 1) was used for geometric optimization, while an irreducible k-point grid of (4 × 1 × 1) together with selected zero-weighted k-points along a high-symmetry path were employed for band structure calculations.

In our recent work,[19] the Perdew−Burke−Ernzerhof (PBE) density functional[27] within the generalized gradient approximation (GGA) was used to generate the ground-state potential energy surface (PES), which described the adiabatic energy transfer channel well. However, it is well-known that GGA-based density functionals often underestimate bandgaps of semiconductors owing to self-interaction errors.[28,29] Indeed, we found that PBE predicts a near-zero band gap for a clean Ge surface. With a moderate increase of computational cost, we obtained a finite band gap of 0.32 eV of the Ge(111)$c(2 \times 8)$ surface by using a meta-GGA-based made simple (MS2)[30] functional. Interestingly, based on the MS2-optimized surface structure, we found that the hybrid HSE06[31] functional yields a comparable band gap of 0.35 eV. This value further increases to 0.57 eV when the surface structure was optimized by HSE06, which is very close to the experimental value[20] (0.49 ± 0.03 eV at 30 K), at the price of being much more expensive than MS2. In addition, the optimized lattice constant by MS2 is 5.688 Å, agreeing well with the experimental value (5.658 Å[32]). As a result, unless explicitly stated otherwise, the MS2 functional was chosen for subsequent NAMD calculations for its good balance between accuracy and efficiency. The experimental lattice constant was applied to be consistent with the PBE-based PES.[19] The MS2-based and HSE06-based band structures will be compared and discussed in more detail along with Figure 2 below.

A quantitative treatment of the nonadiabatic dynamics of surface scattering process is extremely challenging. Indeed, an accurate determination of a manifold of excited states of this periodic system is currently not feasible. Furthermore, the explicit evolution of the system along the nuclear and electronic degrees of freedom in a fully coupled way is even more formidable. In this work, we will focus on the response of the substrate electronic structure to the impact of the H atom at different surface sites, an approach which is aimed at uncovering the mechanism of the interband transition. The case of D

https://doi.org/10.1021/jacsau.4c00909
JACS Au 2024, 4, 4518−4526

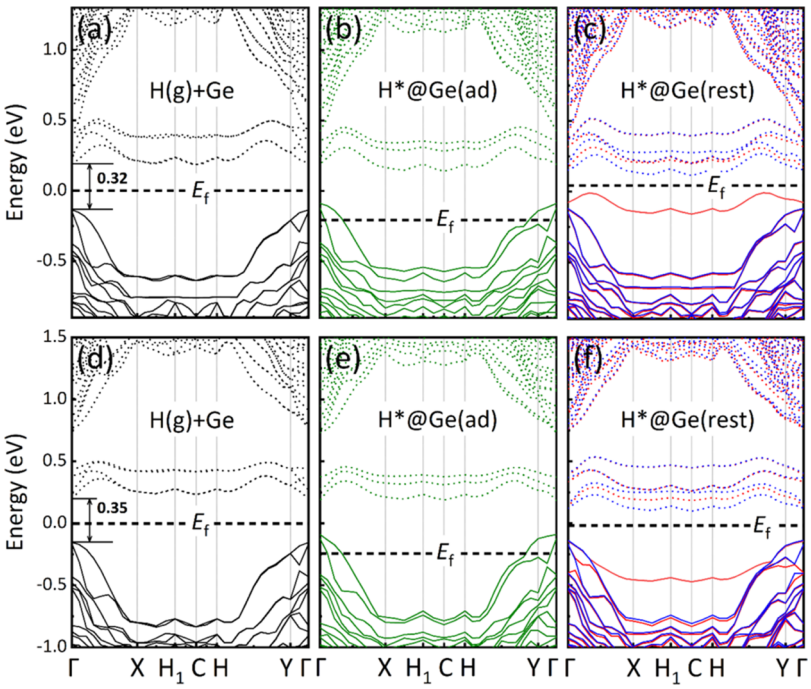

Figure 2. Comparison of the band structures of the Ge(111)$c(2 \times 8)$ surface with H(g) being 6 Å above (H(g)+Ge, left), H adsorbing on the Ge adatom (H*@Ge(ad), middle), and the Ge rest-atom (H*@Ge(rest), right), optimized by the MS2 (a−c) and HSE06 density functionals (d−f). Solid (dotted) lines represent occupied (unoccupied) energy levels. Fermi levels (E_f) are indicated by horizontal black dashed lines and the original bandgaps of the Ge(111)$c(2 \times 8)$ surface are marked by vertical arrows (in eV). Spin-up and spin-down band structures are identical for the H(g)+Ge and H*@Ge(ad) cases, but not for the H*@Ge(rest) case, which are distinguished by blue and red colors, respectively.

scattering is not considered in this work, as the change of projectile mass is not expected to qualitatively alter the electron dynamics. A mixed quantum-classical strategy is used, in which the electronic degrees of freedom are treated quantum mechanically, while the nuclear motion classically. Specifically, we chose an approximate NAMD approach that solves the time-dependent Kohn−Sham (TDKS) equation at the one-electron orbital level based on the surface hopping algorithm[2] and the classical path approximation (CPA).[33−35] This approach has been widely used in combination with ground-state ab initio molecular dynamics (AIMD) to study real-time photoexcited carrier dynamics in condensed phase materials.[36−40] Here, all NAMD calculations were performed with the Hefei-NAMD program.[38]

Specifically, this approach starts with an ansatz that approximates the energies of many-electron states as uncorrelated single excitations in a selected active space (i.e., energy differences of KS orbitals).[36] Single excitations are allowed only among KS orbitals in this active space to form singly excited determinants, $\Phi_j(\mathbf{r};\mathbf{R})$, which are composed of adiabatic one-electron KS orbitals,[33]

$$\Phi_j(\mathbf{r};\ \mathbf{R}) = \hat{A}[\varphi_{j_1}(1)\varphi_{j_2}(2)...\varphi_{j_N}(N)] \tag{1}$$

where $\varphi_j(n)$ is the adiabatic KS orbital ($i = 1,\cdots, N$) dependent on the coordinates of the nth electron, N is the number of the KS orbitals included in the active space, and $\hat{A}$ denotes the antisymmetrization operator. $\Phi_j(\mathbf{r};\mathbf{R})$ is explicitly dependent on the electronic coordinates, $\mathbf{r}$, with a parametric dependence on the nuclear coordinates, $\mathbf{R}$. The electronic wave function, $\Psi_e(\mathbf{r},\ \mathbf{R},\ t)$, is thus expanded as a linear combination of these determinants, respectively.

$$\Psi_e(\mathbf{r},\ \mathbf{R},\ t) = \sum_j c_j(t)\Phi_j(\mathbf{r};\ \mathbf{R}) \tag{2}$$

Inserting eq 2 into the TD Schrödinger equation leads to a set of differential equations,

$$i\hbar\frac{\partial c_j(t)}{\partial t} = \sum_k c_k(t)[\varepsilon_k\delta_{jk} - i\hbar\sigma_{jk}(t)] \tag{3}$$

where ε_k is the excitation energy of the kth eigenstate, σ_{jk} is the time derivative coupling (TDC) between Slater determinants Φ_j and Φ_k, Since we are using one-electron KS orbitals as basis functions, σ_{jk} is nonzero only for pairs of configurations that differ by no more than one KS orbital. As a result, σ_{jk} can be replaced by the coupling between the two KS orbitals (say $\varphi_{k'}$ and $\varphi_{k''}$) differing in the configurations of Φ_j and Φ_k, namely,[38]

$$\begin{aligned}\sigma_{jk} &= \langle\varphi_{k'}\left|\frac{\partial}{\partial t}\right|\varphi_{k''}\rangle \\ &\approx \frac{\langle\varphi_{k'}(t)|\varphi_{k''}(t+\Delta t)\rangle - \langle\varphi_{k'}(t+\Delta t)|\varphi_{k''}(t)\rangle}{2\Delta t}\end{aligned} \tag{4}$$

which is evaluated by a finite difference method.[41]

The CPA further assumes that the nuclear motion is governed by the ground state PES, unaffected by the electronic dynamics. The electronic dynamics along a given classical path of nuclei can be initiated from different electronic configurations, during which the single-electron hopping probabilities between these KS states can then be obtained according to Tully's fewest-switches algorithm,[2]

$$P_{j\to k}(t,\ \Delta t) = \frac{2\Re[c_j^* c_k \sigma_{jk}]\Delta t}{c_j^* c_j} \tag{5}$$

where $\Re$ takes the real part of the quantity in the parentheses. Since we are considering transient electronic excitations during a non-equilibrium collisional process, the Boltzmann factor to maintain the detailed balance was not imposed.[36] It is important to recognize that this ansatz does not properly describe the coupled electron−nuclear dynamics as there is no feedback to the nuclear motion from the electronic dynamics. Specifically, it fails to consider how the nuclear trajectory of the entire system changes after VB-CB excitation compared to the ground state. As a result, our results cannot be quantitatively compared with experimental data. As shown below,

https://doi.org/10.1021/jacsau.4c00909
JACS Au 2024, 4, 4518−4526

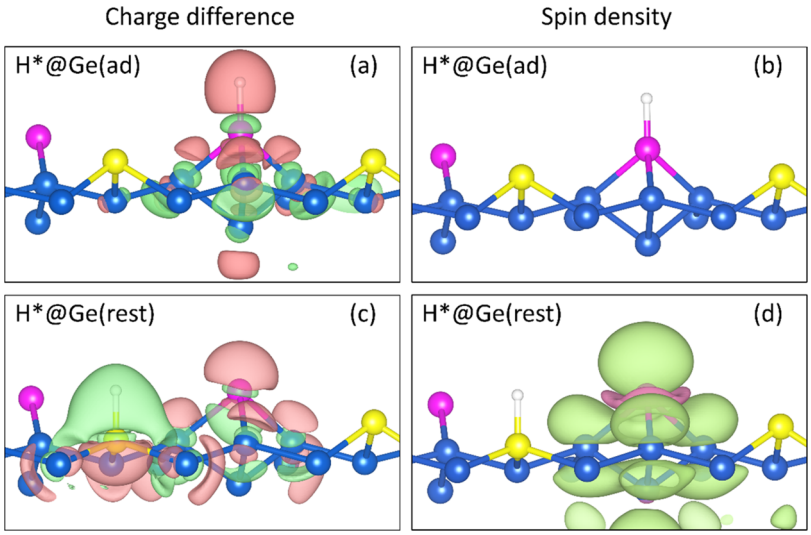

Figure 3. Differential charge density (a, c) and spin density (b, d) distributions of the H*@Ge(ad) and H*@Ge(rest) configurations. Positive values (gaining electrons or spin-up) are shown in pink and negative values (losing electrons or spin-down) in green. Iso-values are 0.007 eV/Å^3 for charge density and 0.0005 au for spin density. Only the Ge atoms of the first layer and above are shown for clarity. Note the relaxed surface structure of the adsorption configuration, rather than the bare surface equilibrium, is taken as the reference geometry for evaluating the charge and spin differences.

however, it is sufficient to qualitatively reveal the impact of the hyperthermal H on the substrate electronic structure and the potential mechanism for nonadiabatic transitions.

In practice, several representative MD trajectories on a previously constructed neural network PES[19] were selected to describe the H atom scattering off the Ge(111)$c(2 \times 8)$ surface at different surface sites at a normal incidence energy (E_i) of 0.99 eV, a representative E_i used in the experiment.[19] The propagations of these trajectories were efficiently carried out using the high-dimensional NN PES and the total energy is well converged within ∼2 meV (Figure S1 in Supporting Information (SI)). Along each trajectory, single point DFT calculations were reperformed at the MS2 level at selected snapshots every 0.5 fs to get the KS orbitals and associated TDCs with a single Γ point. After that, stochastic surface hopping processes were initiated with one electron filling in the valence band maximum (VBM) and then propagated along the selected nuclear trajectory with a step size of 1/1000 of that of AIMD, allowing electron excitation/de-excitation among 50 orbitals below and above the Fermi level. We focus on the electron dynamics from VBM to CBs and exclude the unphysical population transfer from VBM to lower VBs. Due to the stochastic nature of the surface hopping algorithm, the final electronic state populations of different surface hopping events are not expected to be the same. To converge the stochastic surface hopping processes, 20,000 electronic trajectories were conducted for each site to yield the evolution of electronic populations in different orbitals, providing useful information on the electron dynamics.

III. RESULTS AND DISCUSSION

First, let us consider a static description of electronic structures of the Ge(111)$c(2 \times 8)$ surface with and without hydrogen adsorption. In a bare surface, as shown in Figure 1, the Ge adatoms (magenta) and the Ge rest atoms (yellow) are bound to three saturated atoms of the first layer (blue), both featuring a single dangling bond. The saturated atoms are tetrahedrally coordinated and have no unpaired valence electrons. Accordingly, the H atom preferably adsorbs on a Ge rest atom with a binding energy of 2.77 eV (which is defined as the energy of the adsorbed configuration minus that of a H atom being 6 Å above a clean surface), followed by on a Ge adatom (2.25 eV), and on a Ge saturated atom (2.06 eV), at the MS2 level. Since the rest and adatoms pucker a little out of the surface and have a stronger attraction to the H atom, they cast a "shadow" over the saturated atoms, preventing the impinging H atom from directly colliding with latter to a large extent. Consequently, the H atom directed toward the saturated atom will likely be steered to adjacent rest and adatoms during the approach to the surface. In practice, we found it more difficult to select a direct scattering trajectory from a saturated atom than from a rest atom and adatom without being affected by other neighboring atoms. Indeed, we find that merely 8% MD trajectories with our NN PES can be recognized as a single collision of the H atom at saturated atoms with E_i = 0.99 eV, due to this "shadowing" effect, even though the proportion of saturated atoms is much higher than others on the surface. Therefore, we shall focus on the rest and adatoms subsequently. As a signature of the dynamical steering effect, interestingly, the probability of the direct collision on the saturated atom decreases (increases) with the decreasing (increasing) E_i. We would expect a more important role of the saturated atoms in the scattering process at higher incidence energies, which will be studied in the future.

Figure 2 compares the calculated band structures of the pristine Ge(111)$c(2 \times 8)$ surface (H(g)+Ge), H adsorbed on a Ge adatom (H*@Ge(ad)), and on a Ge rest atom (H*@Ge(rest)) using the MS2 and HSE06 functionals, respectively. In both cases, the Ge(111)$c(2 \times 8)$ surface is predicted to have a finite band gap or energy difference between VBM and the conduction band minimum (CBM), 0.32 eV for MS2 and 0.35 eV for HSE06. It is encouraging that the band structures obtained by the two density functionals are quite similar, except for H*@Ge(rest). Note however that the HSE06 results shown here were obtained using the MS2-optimized geometries for computational efficiency. Results with the HSE06-optimized geometries (at a much higher expense) are shown in Figure S2, in which the band structure of H*@Ge(rest) is more consistent with the MS2 result with the spin-down VBM manifesting a similarly weak dispersion around the Γ point. Other site-specific features of band structures are generally unchanged except for a unified lifting of the band

https://doi.org/10.1021/jacsau.4c00909
JACS Au 2024, 4, 4518−4526

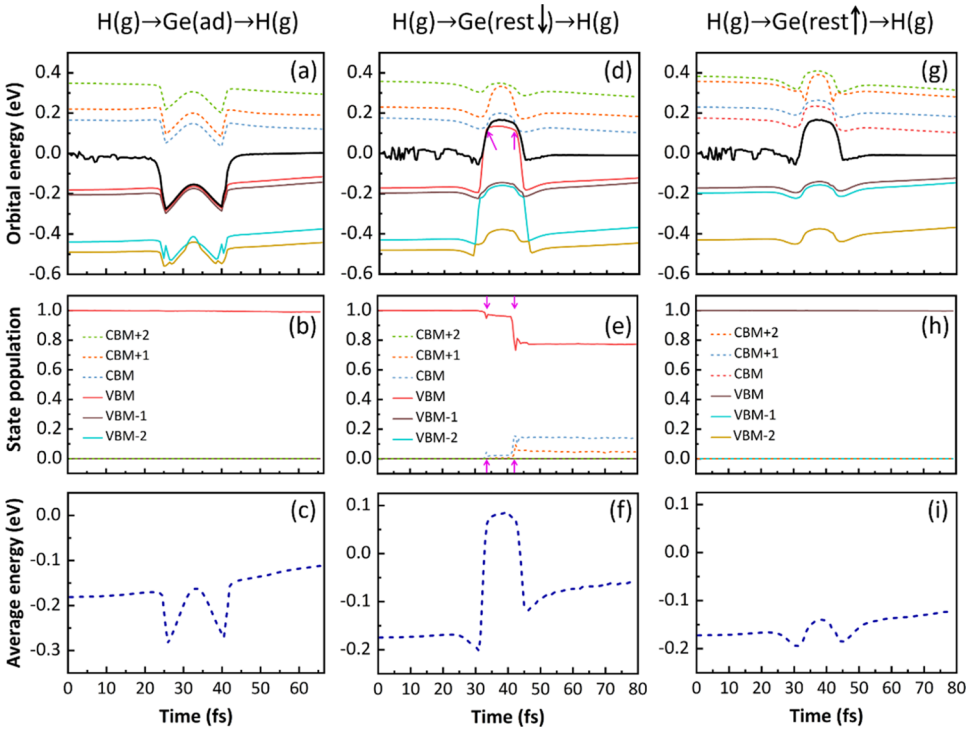

Figure 4. Time evolutions of the KS eigen-energies at the Γ point, the electronic populations of these energy levels near the Fermi level and the average electronic energy of the electronic trajectories of H atom scattering from the adatom (a−c) and the rest atom (d−f) for the spin-down and (g−i) for the spin-up eigenstates) of Ge(111)c(2 × 8) with an electron initially placed in the VBM and E_i = 0.99 eV. Energy levels in the VB (CB) are given in solid (dotted) curves and labeled by their relative sequence to the VBM (CBM). In panels (a), (d), and (g), the Fermi levels are marked by the black solid lines. Pink arrows in panels (d) and (e) indicate the positions of avoided crossings where the electronic transitions occur. Note that the unphysical electronic transition from VBM to VBM-1 and VBM-2 has been excluded. Note the average electron energies are calculated by $\sum_i^N \varepsilon_i \cdot w_i$, where w_i is the population of the ith KS orbital.

gap, as already mentioned in the Methods. This comparison validates the accuracy of MS2 in describing the band structure of this system. According to the analysis of the projected density of states (PDOSs) in Figure S3, we find that the highest VBs (−1−0 eV) are mainly contributed by the rest atoms, while the lowest CBs (0−1 eV) are more related to the adatoms, which is consistent with previous theoretical[42] results and experimental[43] observations.

We next discuss in more detail how the adsorption of an H atom influences the local electronic structure at different surface sites. As the Fermi level of the Ge surface is mostly related to surface states rather than bulk states of the semiconductor, the adsorption of a single H atom can significantly change the Fermi level of the substrate and the PDOSs of relevant Ge atoms, as clearly shown in Figure S3. When a hydrogen atom adsorbs on a Ge adatom, one of the lowest CBs mainly consisting of the unoccupied p_z orbitals of this Ge atom become hybridized with the 1s orbital and filled by the electron of the adsorbed hydrogen atom, leading to a lowering of the Fermi energy (Figures 2b,e and S3b) and making the VBs partially occupied. The change of Fermi level due to the adsorption of a hydrogen atom is not surprising, as also observed in a semiconductor MoO_3, though in an opposite way, because the CB edge becomes partially occupied by doping the H atom in that case.[44] The relative downshift of Fermi energy is ∼0.2 eV using MS2 and ∼0.23 eV with HSE06. In contrast to this, the H−Ge bond formation at the rest atom involves interaction with the fully occupied VB. Consequently, the hybridization of the H atom 1s orbital with the Ge (rest) orbitals, necessary to form a covalent bond, involves transfer of an electron to another originally unoccupied orbital of a dangling bond on the nearest adatom, resulting in the presence of a new VBM.[43] This behavior corresponds to the transfer of PDOSs from the rest atom to the nearest adatom right below the Fermi level in Figure S3c.

The site-dependent electronic structures can be also clearly seen in Figure 3, where the charge density difference between the pristine surface and the surface with an H atom bonding to an adatom and a rest atom is shown. Also shown in Figure 3 are the corresponding spin density distributions. For hydrogen adsorption on the rest atom, it is evident that the H atom loses its electron, which transfers to an adatom next to the rest atom where the hydrogen atom attaches. This reverse charge transfer phenomenon was observed in earlier scanning tunneling microscope images.[42,43] More interestingly, since the H atom brings only one additional electron, the filled orbital of a dangling bond on the adatom (the new VBM) is present only in one spin manifold, as seen in Figures 2c,f and S3c. It is further verified in Figure 3d that a strong spin density only appears on this adatom. This dramatic change sets the stage for the curve crossing discussed below. On the other hand, no such indirect charge transfer is observed when the H atom binds to the adatom, see Figure 3a, suggesting that a crossing of electronic states is less likely (*vide infra*). It is shown that the H−Ge bond formed with the adatom enriches electrons on the H atom and borrows some electron density from nearby saturated Ge atoms. Additionally, there is no net spin density at this configuration (Figure 3b), confirming that the hydrogen adsorption on the adatom does not violate the spin-degeneracy, consistent with Figures 2b,e and S3b. The

https://doi.org/10.1021/jacsau.4c00909
JACS Au 2024, 4, 4518−4526

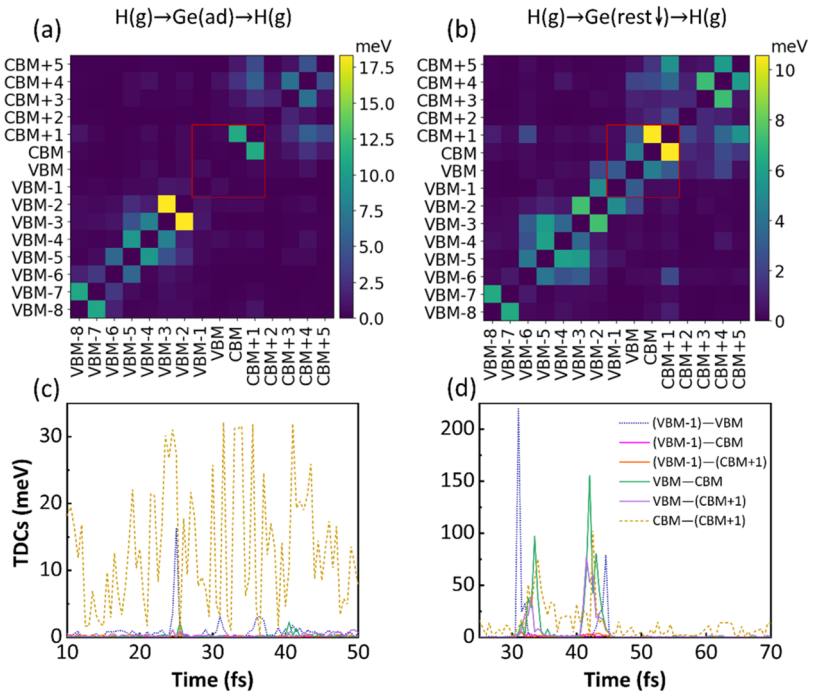

Figure 5. Time-averaged TDC matrices among different orbitals during the H atom scattering from the adatom (a) and rest atom (b) of Ge(111) $c(2 \times 8)$, where the orbitals are labeled by their sequence relative to VBM and CBM, respectively. TDC elements involving these orbitals near the Fermi level are highlighted in the red square and corresponding time-dependent values are presented in panels (c) and (d). Note for the rest atom that the TDCs among spin-down eigenstates are shown only and all TDCs are calculated by $\sum_i^{N_{\text{step}}} \sigma_{jk} \cdot \frac{1000\hbar}{2N_{\text{step}}}$, where N_{step} is the total number of time steps and 1000 is a factor for converting the unit to meV.

comparison clearly underscores the drastic differences in the local electronic structures for H adsorption at different surface sites.

We next study the electronic dynamics of the hydrogen atom colliding at two surface sites of the Ge(111)$c(2 \times 8)$ surface by initially placing an electron in the VBM. Two exemplary scattering trajectories are illustrated in Figure 1. The corresponding time evolutions of the KS eigen-energies at the Γ point, the electronic populations of these eigenstates near the Fermi level, and the average electronic energy are shown in Figure 4. To simplify the problem, here the incident H atom is directed toward the specified site initially along the surface normal from 6 Å above the surface and the initial surface temperature is set to 0 K to avoid mixing of KS orbitals caused by the thermal motion of surface atoms. During this process, the hydrogen impact only affects the Ge atoms within a small range, and there is no interaction between the neighboring supercells. Consequently, using only the Γ point should be sufficient to capture the site-dependent electronic structure. In addition, the VBM and lowest CBs are relatively flat for the H*@Ge(rest), the only site that triggers nonadiabaticity. Furthermore, we have calculated the electron density of states with a dense grid of k-points $(8 \times 2 \times 1)$ and compared its projection on the Γ point with that calculated with a single Γ point. As shown in Figure S4, the two results agree with each other very well. This indicates that the dispersion of VB does not affect the electron density of states at the Γ point. It is thus reasonable to discuss the electron dynamics at the Γ point only. Note that the electron transfer effect on the local structure around the adsorbed H atom is considered in the ground state trajectory. Since the scattering process is fast with a time scale on the order of dozens of femtoseconds and small energy gaps, decoherence is not considered important in this process.[34] Due to these limitations, this model is by no means a faithful representation of the experiment, it nevertheless provides insight into how the nuclear motion affects the electronic energy and transitions.

For the collision at the adatom site, as shown in Figure 4a–c, the KS orbitals exhibited a synchronized lowering of their energies, as H approaches the surface reaching its distance of closest approach at about 25 fs. The system largely recovers when H departs after 40 fs. Importantly, overall, the order of the KS orbitals is almost kept the same and no near degeneracies arise between VB and CB states. The band gap remains throughout the scattering. As shown in Figure 4b, the occupancy of VBM is kept at one, while all other orbitals are essentially unoccupied throughout, indicating that no electronic transition takes place. The average electronic energy, which is calculated by summing the energies of all electronic states weighted by their relative populations, shows two pronounced dips in Figure 4c, reflecting the lowering of the KS energies (particularly that of VBM) as H forms a bond with the adatom. Overall, the incoming and outgoing average electronic energies are only slightly different due to the small energy change of the adiabatic KS orbitals, which is irrelevant to nonadiabatic transitions.

The situation is drastically different for H impinging on the rest atom. Note in this case that avoided crossings are present for one manifold of spin states, while absent in the other, as expected from the band structure of H*@Ge(rest) in Figure 2 (where spin–orbit coupling is neglected). For the spin manifold with strong nonadiabatic characteristics (spin-down here), Figure 4d shows that VBM first undergoes an avoided crossing with VBM-1 and VBM-2 at ∼30 fs as the H projectile

https://doi.org/10.1021/jacsau.4c00909
JACS Au 2024, 4, 4518–4526

approaches the surface and then steadily rises in energy by more than 0.3 eV at 33 fs, and more importantly, becomes near-degenerate with the CBM. This increase in energy is close to the band gap of the pristine Ge surface, leading to the absence of a band gap at the crossing point. The near-degeneracy reappears at 41 fs as H departs the surface and re-enters this curve-crossing area. In the meantime, there are some other avoided crossings between other KS orbitals, e.g., CBM and CBM+1. As a result, we observe an increasing population in CBM and CBM+1 at 33 and 41 fs, indicating an interband nonadiabatic transition. Accordingly, the average electronic energy climbs dramatically as the H atom approaches the rest atom, as seen in Figure 4f. In contrast, Figure 4g shows clearly in the other spin manifold (spin-up here), these KS orbital energy curves in the VB and CB do not cross at all. Consequently, electronic transitions are unlikely (Figure 4h) and the mean electronic energy varies only modestly (Figure 4i), analogously with the energy of VBM. We note however that the inclusion of the spin−orbit coupling may allow electronic transitions between different spin states.

We can further relate the site-specific electron dynamics of the H collision to the TDCs along the electronic trajectories. Figure 5 compares time-dependent and time-averaged TDCs over all snapshots of electronic trajectories for H scattering from the adatom and from the rest atom (for the spin-down manifold with strong couplings only). It is clear that for the H atom collision at the adatom site, the KS orbitals above and below the Fermi level have negligibly small couplings. The largest TDC is found between VBM-3 and VBM-2 (see Figure 5a), which are deep in the VB but should have little impact on the nonadiabatic interband transitions from VB to CB. Consequently, no electronic excitations from VB to CB are seen in this process. In contrast, for the H atom collision at the rest atom, the TDCs are on average much larger and more widely distributed among these orbitals near the Fermi level. Specifically, the TDCs between VBM-1 and VBM, VBM and CBM, CBM and CBM+1, increase sharply when the KS orbitals undergo avoided crossings around 30 and 40 fs, indicating high probabilities of nonadiabatic transitions at these snapshots. This physical picture is fully consistent with that shown in Figure 4, corresponding to the changes of electronic populations in these orbitals. We note in passing that the TDCs between CBM and CBM+1 are also large for the adatom site near 25 fs. While CBM is unoccupied at low temperatures, it can be thermally populated at elevated temperatures. Furthermore, one can also populate CBM by n-doping in a semiconductor sample. In such cases, the transitions between CBM and CBM+1 could become relevant, for example, to recent surface temperature-dependent scattering experiments.[45]

It is worth mentioning that the transient near degeneracies between VBM and CBM observed here along the trajectories are analogous to avoided crossings between different electronic states in a gaseous system. The drastic changes in the KS energies in a very localized region are obviously caused by the strong perturbation of the electronic structure by the collision of the hyperthermal H atom. With sufficient collision energy, the impinging H pushes the system to reach a sufficiently high electronic energy, thus allowing the transition of a surface electron from the VB to the CB. The newly created high-energy EHP may dissipate its energy quickly to the Ge substrate and the rebounding H atom loses a significant portion of its kinetic energy, as observed in the experiment. The observed site-specific nonadiabatic effects also provide a qualitative interpretation to the experimental observation for the similar measured nonadiabatic energy loss spectra of H and D atoms scattered from Ge(111)$c(2 \times 8)$.[21] This observation can be understood, if the nonadiabatic transition only occurs near the rest atom site. In such a case, both D and H atoms can excite electrons from VB to CB, regardless their velocity difference at the same incidence energy, thus leading to the absence of an isotope effect.

Overall, using the CPA-NAMD approach, we have provided the qualitative first-principles interpretation to experimental observations for hydrogen scattering from Ge(111)$c(2 \times 8)$ and additional insights about the site-specific nonadiabatic effect. Such a detailed level of understanding cannot be obtained by the EF theory, which only approximates the delocalized and low-energy electronic excitation within a continuum of excited states as a dragging force to nuclei but fails to account for explicit electronic excitation from the VB to the CB overcoming a finite gap. Admittedly, the main limitation of the CPA is that there is no feedback to the nuclear motion from the electronic dynamics, which prevent us from gaining the energy loss profile to be quantitively compared with experiment. The lack of nuclear-electronic feedback can of course affect the electron dynamics to some extent, for example, on the precise time and position where electronic transition would occur. However, we believe that our observation on the site-specific nonadiabatic dynamics is largely determined by the perturbation of the local electronic structure by the impinging H atom, which would not be significantly altered by this approximation. Another source of uncertainty of our dynamics results is the influence of the density functional. Here, the ground state PBE-based PES is less crucial provided that the selected trajectory involves direct scattering from the same surface atom, where the electron dynamics should be similar. Of course, using a more accurate functional, like HSE06, to run the NAMD dynamics may change the results of the current simulations to some extent. But this should be a minor change, as the band structures by MS2 and HSE06 are very similar except the somewhat larger band gap of the latter. More sophisticated electronic structure and nonadiabatic dynamics theories are needed in the future to quantify the nonadiabatic effects in this system.

IV. CONCLUSIONS

Recent experimental exploration of gas-surface scattering has uncovered various nonadiabatic phenomena. Many such phenomena at metal surfaces can be framed within an electronic friction model in which thermal excitation of electron−hole pairs leads to a frictional force for the nuclear motion. However, such a friction model becomes inadequate for collisions from semiconductor surfaces, which have significant bandgaps. In recent experimental studies of H atom scattering from a reconstructed Ge(111)$c(2 \times 8)$ surface, significant energy losses were observed and attributed to a nonadiabatic transition of a surface electron from its valence band to conduction band. In this work, we present a mixed quantum-classical model to examine the collision-induced nonadiabatic dynamics and its site specificity, in which the quantum electronic degrees of freedom are modeled by single-electron Kohn−Sham orbitals with classical nuclear motion within the classical path approximation.

Our nonadiabatic molecular dynamics simulations revealed significant collision-induced perturbation of the Kohn−Sham

https://doi.org/10.1021/jacsau.4c00909
JACS Au 2024, 4, 4518−4526

orbitals, leading to electronic transitions from the valence band to the conduction band. Specifically, the high kinetic energy of the impinging H atom enables the access of high-energy near degeneracies between Kohn−Sham orbitals that are normally separated by the large band gap, resulting in the conversion of nuclear kinetic energy to electronic energy and ultimately the significant slowdown of the scattered H atom observed in the experiment. Such nonadiabatic transitions are possible at the rest atom site of the Ge surface and only in a particular spin manifold, but not at the adatom site, confirming our earlier speculations. This dramatic site specificity in nonadiabatic dynamics can be traced back to the different local band structures perturbated by the approach of the energetic H atom at these sites. The site specificity of nonadiabatic transitions might have important implications in an array of fields including semiconductor device fabrication. It also provides a useful construct for future development of more quantitative models for nonadiabatic processes on surfaces.

■ ASSOCIATED CONTENT

Supporting Information

The Supporting Information is available free of charge at https://pubs.acs.org/doi/10.1021/jacsau.4c00909.

Computational details of the NN PES; Additional results on the energy conservation, band structures, projected density of states, and optimized geometries (PDF)

■ AUTHOR INFORMATION

Corresponding Authors

Jin Zhao − *Key Laboratory of Precision and Intelligent Chemistry, University of Science and Technology of China, Hefei, Anhui 230026, China; Department of Physics, University of Science and Technology of China, Hefei, Anhui 230026, China;* orcid.org/0000-0003-1346-5280; Email: zhaojin@ustc.edu.cn

Hua Guo − *Department of Chemistry and Chemical Biology, Center for Computational Chemistry, University of New Mexico, Albuquerque, New Mexico 87131, United States;* orcid.org/0000-0001-9901-053X; Email: hguo@unm.edu

Bin Jiang − *Key Laboratory of Precision and Intelligent Chemistry, University of Science and Technology of China, Hefei, Anhui 230026, China; Department of Chemical Physics, University of Science and Technology of China, Hefei, Anhui 230026, China;* orcid.org/0000-0003-2696-5436; Email: bjiangch@ustc.edu.cn

Authors

Lingjun Zhu − *Key Laboratory of Precision and Intelligent Chemistry, University of Science and Technology of China, Hefei, Anhui 230026, China; Department of Chemical Physics, University of Science and Technology of China, Hefei, Anhui 230026, China*

Qijing Zheng − *Key Laboratory of Precision and Intelligent Chemistry, University of Science and Technology of China, Hefei, Anhui 230026, China; Department of Physics, University of Science and Technology of China, Hefei, Anhui 230026, China;* orcid.org/0000-0003-0022-3442

Yingqi Wang − *Department of Chemistry and Chemical Biology, Center for Computational Chemistry, University of New Mexico, Albuquerque, New Mexico 87131, United States*

Kerstin Krüger − *Institute of Physical Chemistry, Georg-August University, Göttingen 37077, Germany;* orcid.org/0000-0002-5826-2674

Alec M. Wodtke − *Institute of Physical Chemistry, Georg-August University, Göttingen 37077, Germany; Department of Dynamics at Surfaces, Max-Planck-Institute for Multidisciplinary Sciences, Göttingen 37077, Germany; International Center of Advanced Studies of Energy Conversion, Georg-August University, Göttingen 37077, Germany;* orcid.org/0000-0002-6509-2183

Oliver Bünermann − *Institute of Physical Chemistry, Georg-August University, Göttingen 37077, Germany; Department of Dynamics at Surfaces, Max-Planck-Institute for Multidisciplinary Sciences, Göttingen 37077, Germany; International Center of Advanced Studies of Energy Conversion, Georg-August University, Göttingen 37077, Germany;* orcid.org/0000-0001-9837-6548

Complete contact information is available at: https://pubs.acs.org/10.1021/jacsau.4c00909

Notes

The authors declare no competing financial interest.

■ ACKNOWLEDGMENTS

This work is mainly supported by the Strategic Priority Research Program of the Chinese Academy of Sciences (XDB0450101 to B.J. and J.Z.), the National Natural Science Foundation of China (22325304 and 22221003 to B.J.), and the US NSF (grant no. CHE-2306975 to H.G.). The Alexander von Humboldt Foundation to H.G., O.B., and A.M.W. acknowledge support from the Deutsche Forschungsgemeinschaft (DFG) under grant no. 217133147 (SFB1073, project A04) and from the DFG, the Ministerium für Wissenschaft und Kultur, Niedersachsen and the Volkswagenstiftung under grant no. 191331650. A.M.W. thanks the Max Planck Society for the advancement of science. B.J. and H.G. also thank Prof. Wei Hu and Prof. Oleg Prezhdo, respectively, for some stimulating discussions. We thank the Supercomputing Center of USTC, Hefei Advanced Computing Center, Beijing PARATERA Tech CO., Ltd for providing high-performance computing service.

■ REFERENCES

(1) Born, M.; Huang, K. *Dynamical Theory of Crystal Lattices*; Clarendon: Oxford, 1954.

(2) Tully, J. C. Molecular dynamics with electronic transitions. *J. Chem. Phys.* **1990**, *93* (2), 1061−1071.

(3) Jasper, A. W.; Dawes, R. Non-Born−Oppenheimer molecular dynamics of the spin-forbidden reaction $O(^3P) + CO(X^1\sum^+) \rightarrow CO_2(\tilde{X}^1\sum_g^+)$. *J. Chem. Phys.* **2013**, *139* (15), No. 154313.

(4) Guo, H.; Yarkony, D. R. Accurate nonadiabatic dynamics. *Phys. Chem. Chem. Phys.* **2016**, *18*, 26335−26352.

(5) Subotnik, J. E.; Jain, A.; Landry, B.; Petit, A.; Ouyang, W.; Bellonzi, N. Understanding the Surface Hopping View of Electronic Transitions and Decoherence. *Annu. Rev. Phys. Chem.* **2016**, *67* (1), 387−417.

(6) Curchod, B. F. E.; Martínez, T. J. Ab initio nonadiabatic quantum molecular dynamics. *Chem. Rev.* **2018**, *118* (7), 3305−3336.

(7) Shu, Y.; Varga, Z.; Kanchanakungwankul, S.; Zhang, L.; Truhlar, D. G. Diabatic States of Molecules. *J. Phys. Chem. A* **2022**, *126* (7), 992−1018.

(8) Wu, Q.; Zhou, L.; Schatz, G. C.; Zhang, Y.; Guo, H. Mechanistic Insights into Photocatalyzed H2 Dissociation on Au Clusters. *J. Am. Chem. Soc.* **2020**, *142* (30), 13090−13101.

(9) You, P.; Chen, D.; Lian, C.; Zhang, C.; Meng, S. First-principles dynamics of photoexcited molecules and materials towards a quantum description. *WIREs Comput. Mol. Sci.* **2021**, *11* (2), No. e1492.
(10) Wodtke, A. M. Electronically non-adiabatic influences in surface chemistry and dynamics. *Chem. Soc. Rev.* **2016**, *45* (13), 3641−3657.
(11) Alducin, M.; Díez Muiño, R.; Juaristi, J. I. Non-adiabatic effects in elementary reaction processes at metal surfaces. *Prog. Surf. Sci.* **2017**, *92* (4), 317−340.
(12) Morin, M.; Levinos, N. J.; Harris, A. L. Vibrational energy transfer of CO/Cu(100): Nonadiabatic vibration/electron coupling. *J. Chem. Phys.* **1992**, *96*, 3950−3956.
(13) Huang, Y.; Rettner, C. T.; Auerbach, D. J.; Wodtke, A. M. Vibrational promotion of electron transfer. *Science* **2000**, *290*, 111−114.
(14) White, J. D.; Chen, J.; Matsiev, D.; Auerbach, D. J.; Wodtke, A. M. Conversion of large-amplitude vibration to electron excitation at a metal surface. *Nature* **2005**, *433* (7025), 503−505.
(15) Diesing, D.; Hasselbrink, E. Chemical energy dissipation at surfaces under UHV and high pressure conditions studied using metal−insulator−metal and similar devices. *Chem. Soc. Rev.* **2016**, *45* (13), 3747−3755.
(16) Bünermann, O.; Jiang, H.; Dorenkamp, Y.; Kandratsenka, A.; Janke, S. M.; Auerbach, D. J.; Wodtke, A. M. Electron-hole pair excitation determines the mechanism of hydrogen atom adsorption. *Science* **2015**, *350* (6266), 1346−1349.
(17) Head-Gordon, M.; Tully, J. C. Molecular dynamics with electronic frictions. *J. Chem. Phys.* **1995**, *103*, 10137−10145.
(18) Wodtke, A. M.; Huang, Y.; Auerbach, D. J. Interaction of NO(v = 12) with LiF(001): Evidence for anomalously large vibrational relaxation rates. *J. Chem. Phys.* **2003**, *118* (17), 8033−8041.
(19) Krüger, K.; Wang, Y.; Tödter, S.; Debbeler, F.; Matveenko, A.; Hertl, N.; Zhou, X.; Jiang, B.; Guo, H.; Wodtke, A. M.; Bünermann, O. Hydrogen atom collisions with a semiconductor efficiently promote electrons to the conduction band. *Nat. Chem.* **2023**, *15* (3), 326−331.
(20) Feenstra, R. M.; Lee, J. Y.; Kang, M. H.; Meyer, G.; Rieder, K. H. Band gap of the Ge(111)c(2 × 8) surface by scanning tunneling spectroscopy. *Phys. Rev. B* **2006**, *73* (3), No. 035310.
(21) Krüger, K.; Wang, Y.; Zhu, L.; Jiang, B.; Guo, H.; Wodtke, A. M.; Bünermann, O. Isotope effect suggests site-specific non-adiabaticity on Ge(111)c(2 × 8). *Nat. Sci.* **2024**, *4* (1), No. e20230019.
(22) Dorenkamp, Y.; Jiang, H.; Köckert, H.; Hertl, N.; Kammler, M.; Janke, S. M.; Kandratsenka, A.; Wodtke, A. M.; Bünermann, O. Hydrogen collisions with transition metal surfaces: Universal electronically nonadiabatic adsorption. *J. Chem. Phys.* **2018**, *148* (3), No. 034706.
(23) Bünermann, O.; Kandratsenka, A.; Wodtke, A. M. Inelastic Scattering of H Atoms from Surfaces. *J. Phys. Chem. A* **2021**, *125* (15), 3059−3076.
(24) Hertl, N.; Maurer, R. J. Energy transfer during hydrogen atom collisions with surfaces. *Trends Chem.* **2023**, *5* (11), 795−798.
(25) Kresse, G.; Hafner, J. Ab initio molecular dynamics for liquid metals. *Phys. Rev. B* **1993**, *47*, 558−561.
(26) Blöchl, P. E. Projector augmented-wave method. *Phys. Rev. B* **1994**, *50*, 17953−17979.
(27) Perdew, J. P.; Burke, K.; Ernzerhof, M. Generalized gradient approximation made simple. *Phys. Rev. Lett.* **1996**, *77*, 3865−3868.
(28) Perdew, J. P.; Levy, M. Physical Content of the Exact Kohn-Sham Orbital Energies: Band Gaps and Derivative Discontinuities. *Phys. Rev. Lett.* **1983**, *51* (20), 1884−1887.
(29) Mori-Sánchez, P.; Cohen, A. J.; Yang, W. Localization and Delocalization Errors in Density Functional Theory and Implications for Band-Gap Prediction. *Phys. Rev. Lett.* **2008**, *100* (14), No. 146401.
(30) Sun, J.; Haunschild, R.; Xiao, B.; Bulik, I. W.; Scuseria, G. E.; Perdew, J. P. Semilocal and hybrid meta-generalized gradient approximations based on the understanding of the kinetic-energy-density dependence. *J. Chem. Phys.* **2013**, *138* (4), No. 044113.
(31) Krukau, A. V.; Vydrov, O. A.; Izmaylov, A. F.; Scuseria, G. E. Influence of the exchange screening parameter on the performance of screened hybrid functionals. *J. Chem. Phys.* **2006**, *125* (22), No. 224106.
(32) Hom, T.; Kiszenik, W.; Post, B. Accurate lattice constants from multiple reflection measurements. II. Lattice constants of germanium silicon, and diamond. *J. Appl. Crystallogr.* **1975**, *8* (4), 457−458.
(33) Craig, C. F.; Duncan, W. R.; Prezhdo, O. V. Trajectory Surface Hopping in the Time-Dependent Kohn-Sham Approach for Electron-Nuclear Dynamics. *Phys. Rev. Lett.* **2005**, *95* (16), No. 163001.
(34) Jaeger, H. M.; Fischer, S.; Prezhdo, O. V. Decoherence-induced surface hopping. *J. Chem. Phys.* **2012**, *137* (22), No. 22A545.
(35) Akimov, A. V.; Prezhdo, O. V. Advanced Capabilities of the PYXAID Program: Integration Schemes, Decoherence Effects, Multiexcitonic States, and Field-Matter Interaction. *J. Chem. Theory Comput.* **2014**, *10* (2), 789−804.
(36) Akimov, A. V.; Prezhdo, O. V. The PYXAID Program for Non-Adiabatic Molecular Dynamics in Condensed Matter Systems. *J. Chem. Theory Comput.* **2013**, *9* (11), 4959−4972.
(37) Long, R.; Prezhdo, O. V.; Fang, W. Nonadiabatic charge dynamics in novel solar cell materials. *WIREs Comput. Mol. Sci.* **2017**, *7* (3), No. e1305.
(38) Zheng, Q.; Chu, W.; Zhao, C.; Zhang, L.; Guo, H.; Wang, Y.; Jiang, X.; Zhao, J. Ab initio nonadiabatic molecular dynamics investigations on the excited carriers in condensed matter systems. *WIREs Comput. Mol. Sci.* **2019**, *9* (6), No. e1411.
(39) Yang, J.-J.; Chen, W.-K.; Liu, X.-Y.; Fang, W.-H.; Cui, G. Spin−Orbit Coupling Is the Key to Promote Asynchronous Photoinduced Charge Transfer of Two-Dimensional Perovskites. *JACS Au* **2021**, *1* (8), 1178−1186.
(40) Sifain, A. E.; Bjorgaard, J. A.; Nelson, T. R.; Nebgen, B. T.; White, A. J.; Gifford, B. J.; Gao, D. W.; Prezhdo, O. V.; Fernandez-Alberti, S.; Roitberg, A. E.; Tretiak, S. Photoexcited Nonadiabatic Dynamics of Solvated Push−Pull π-Conjugated Oligomers with the NEXMD Software. *J. Chem. Theory Comput.* **2018**, *14* (8), 3955−3966.
(41) Billeter, S. R.; Curioni, A. Calculation of nonadiabatic couplings in density-functional theory. *J. Chem. Phys.* **2005**, *122* (3), No. 034105.
(42) Klitsner, T.; Nelson, J. S. Site-specific hydrogen reactivity and reverse charge transfer on Ge(111)-c(2 × 8). *Phys. Rev. Lett.* **1991**, *67* (27), 3800−3803.
(43) Razado, I. C.; Zhang, H. M.; Hansson, G. V.; Uhrberg, R. I. G. Hydrogen-induced metallization on Ge(111) c(2 × 8). *Appl. Surf. Sci.* **2006**, *252* (15), 5300−5303.
(44) Zhu, Q.; Jiang, S.; Ye, K.; Hu, W.; Zhang, J.; Niu, X.; Lin, Y.; Chen, S.; Song, L.; Zhang, Q.; Jiang, J.; Luo, Y. Hydrogen-Doping-Induced Metal-Like Ultrahigh Free-Carrier Concentration in Metal-Oxide Material for Giant and Tunable Plasmon Resonance. *Adv. Mater.* **2020**, *32* (50), No. 2004059.
(45) Krüger, K.; Hertl, N.; Wodtke, A. M.; Bünermann, O. Temperature dependence of the Ge(111) surface electronic structure probed by inelastic H atom scattering. *Phys. Rev. Mater.* **2024**, *8* (3), No. 034603.

https://doi.org/10.1021/jacsau.4c00909
JACS Au 2024, 4, 4518−4526